JOURNAL OF MATERIALS SCIENCE 22 (1987) 2521–2528

The effect of cyclic creep on grain-boundary cavitation in ceramics

R. A. PAGE, J. LANKFORD
Department of Materials Science, Southwest Research Institute, San Antonio, Texas 78284, USA

Small-angle neutron scattering has been used to characterize the cavity distribution in crept samples of a hot-pressed silicon carbide, which contained a thin continuous amorphous phase, and a sintered alumina, which contained no amorphous phase. The compression creep experiments were performed under cyclic loading at 1600° C and a frequency of 0.33 Hz. Comparison of the cavitation rates under cyclic loading with previously measured rates under static loading indicates that cavitation in the silicon carbide was unaffected by the cyclic loading, while the cavity volume fraction and the cavity size in the alumina were slightly increased by the cyclic loading. The results suggest that 0.33 Hz is too slow a frequency to affect the stress distribution and thus cavitation in the glassy phase containing silicon carbide, but it is rapid enough to accelerate cavitation in the absence of a glassy phase. This hypothesis is supported both by experimental results from other ceramic and metal systems and by calculations of characteristic stress relaxation times.

1. Introduction

The utilization of ceramics as high-temperature structural components will necessarily subject the ceramic materials to long-term creep loading. Failure under these conditions is likely to occur by the nucleation, growth, and coalescence of grain-boundary cavities. In addition to the static loading, many applications will also impose some degree of cyclic loading, either due to vibration or start-up shut-down cycles. Studies of metallic materials [1, 2] suggest that differences between the static and cyclic behaviour can exist. Similar studies of the effect of cyclic loading on cavitation in ceramics have not yet been reported.

Any detailed study of cavitation kinetics, at a minimum, requires the measurement of nucleation rates and growth rates such that the nucleation and growth processes, which occur simultaneously, can be separated. Precision density measurements, scanning electron microscopy, and transmission electron microscopy are unsatisfactory for this purpose; precision density measurements cannot separate the nucleation and growth events, scanning electron microscopy using intergranular fracture techniques does not have enough resolution for investigating nucleation and early growth, and transmission electron microscopy of thinned foils does not provide sufficient statistical accuracy because of the very small volume of material examined. Small-angle neutron scattering (SANS), on the other hand, has proved to be a powerful technique for cavitation studies. Saegusa *et al.* [3] and Page *et al.* [4], in the initial studies of grain-boundary cavitation, demonstrated the unique ability of SANS to provide the desired nucleation and growth rates as well as the cavity-size distributions. Since these initial studies, SANS has been successfully utilized to characterize grain-boundary cavitation in a number of metallic [5–7] and ceramic [8–11] systems.

This paper presents the results of a SANS characterization of cavitation in two ceramics subjected to cyclic creep loading. Comparison of these results with those previously reported for static loading [9, 10] provides a means of identifying the effect of periodic loading and unloading on cavitation. The effect of the cyclic component of loading on creep rate is also presented.

2. Experimental details

The objective of this study was to determine the effect of periodic loading and unloading on cavitation kinetics. To accomplish this, the cavitation behaviour of specimens exposed to cyclic loading will be compared to previously reported results obtained under static loading [9, 10]. For this to be a valid comparison it was necessary to duplicate, as closely as possible, the conditions of the earlier creep tests. Thus, the materials, creep testing procedures, and SANS measurement procedures described below are identical to those employed in the previous tests, with the one exception being the use of a cyclic load in the present tests instead of the static load used in the earlier tests.

2.1. Materials

Two relatively simple ceramics, a hot-pressed silicon carbide (NC 203, Norton Company, Worcester, Massachusetts) and a sintered alumina (Lucalox, General Electric Lamp Glass Division, Cleveland, Ohio) were selected for this study. These two ceramics differed from one another in both grain size and grain-boundary microstructure. The hot-pressed silicon carbide had an average grain size of approximately 5 μm. Previous results of TEM, Auger, and microprobe work [10, 12] suggest that a glassy phase rich in aluminium and oxygen was present as a thin continuous grain-boundary film in the silicon carbide.

0022–2461/87 $03.00 + .12

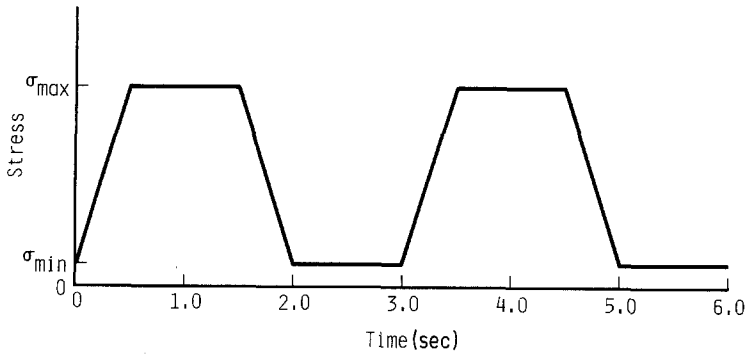

Figure 1 Schematic drawing of loading cycle employed in the cyclic creep tests.

The sintered alumina had an average grain size of approximately 30 μm. Previous detailed studies of its grain-boundary microstructure [13–21] have identified large $MgAl_2O_4$ spinel particles, usually located at triple points, and calcium segregation to the grain boundary, but have failed to identify a grain-boundary glassy phase of either a continuous or discontinuous nature.

2.2. Creep tests

Compression creep specimens were fabricated in the form of right-circular cylinders, 6.4 mm diameter and 1.2 mm long. Specimen ends were ground and lapped flat, and parallel to within 5 μm. Similar preparation was performed on the loading platens, which were fabricated from 12.7 mm diameter rods of sintered α-SiC (Carborundum Company, Niagara Falls, New York). The silicon carbide specimens and the alumina specimens were tested in the as-hot-pressed and as-sintered conditions, respectively.

Cyclic creep testing was performed at 1600° C in a servo-controlled hydraulic test machine equipped with a controlled environment (titanium gettered argon) resistance furnace. The loading cycle (Fig. 1) was made up of a linear ramp of 0.5 sec duration from σ_{min} to σ_{max}, a 1.0 sec hold at σ_{max}, a linear ramp of 0.5 sec duration from σ_{max} to σ_{min}, and a 1.0 sec hold at σ_{min}. The cyclic waveform was thus symmetrical, i.e. the loading and unloading rates were identical as were the hold times at σ_{min} and σ_{max}, with a frequency of 0.33 Hz. The value of σ_{max} was the same as the stress employed in the earlier creep studies [9, 10]: 605 MPa for silicon carbide and 140 MPa for alumina. σ_{min} was kept as low as possible (R = 0.1 for SiC and 0.25 for Al_2O_3, where the stress ratio R is defined as the ratio of the minimum cyclic stress to the maximum cyclic stress, thus for static loading, R = 1.0) while still providing enough load to maintain alignment; σ_{min} = 69 MPa for silicon carbide and 34 MPa for alumina. Cyclic creep tests were run for times ranging from 1.8×10^3 to 2.6×10^5 sec for silicon carbide and 1.8×10^3 to 7.1×10^4 sec for alumina. Once the desired test duration had been achieved, the specimens were rapidly cooled to room temperature while being held at σ_{max}.

2.3. SANS measurements

Following creep, 5 mm × 12.7 mm rectangular flats were ground and polished on opposite sides of the specimens. This procedure yielded specimens approximately 3.7 mm thick, as measured between the parallel flats. Final polishing was performed such that grain pull-out was minimized and a similar surface finish was achieved on each specimen. As-received control samples of each material were prepared in a similar fashion.

The small-angle scattering measurements, which were performed on the 30 m instrument at the National Center for Small-Angle Scattering Research at Oak Ridge National Laboratory, utilized an incident neutron wavelength, λ, of 0.475 nm and sample to detector distances of 9 and 16.5 m. This scattering geometry yielded intensity data at scattering vectors, q, from 0.037 to 0.2 nm^{-1}, where $q = 4\pi \sin\theta/\lambda$ and 2θ is the scattering angle. Parasitic scattering effects arising from electronic background and the empty specimen holder as well as non-uniform detector sensitivity were corrected for as described by Page *et al.* [4]. The corrected data were radially averaged, and then converted to a macroscopic differential scattering cross-section, $d\Sigma/d\Omega$, by calibration in reference to the scattering cross-section of voids in a well-characterized irradiated aluminium sample [22].

3. Data analysis

Small-angle scattering may be produced by a variety of sources, e.g. dislocations, precipitates, grain-boundary glassy phases, surfaces, and cavities. Therefore, before information on cavitation can be obtained from the SANS data it is necessary to remove that portion of the scattered intensity which arises from sources other than cavities. To accomplish this, scattering from an as-received sample is subtracted from that of the crept samples. In this manner, scattering due to dislocations, external surfaces, stable precipitates, and the grain-boundary second phase is removed. Incoherent scattering is also eliminated by this subtraction; what remains is solely the scattered intensity produced by the creep process. If the precipitates and grain-boundary second phase are stable at the test temperature, then it can be correctly assumed that the scattered intensity produced by creep is the result of cavity nucleation and growth alone. This has been shown to be the case for both of the materials used in this study [9, 10]. Hence, in all data analysis procedures, the scattered intensity resulting from creep is assumed to originate entirely from cavities.

Standard methods for analysing small-angle scattering data were used to determine the radius of gyration, R_G, the Porod radius, R_p, the cavity volume per unit volume, V_c/V, and the number of cavities per unit volume, N_c/V. The equations employed in the analyses are presented in the Appendix.

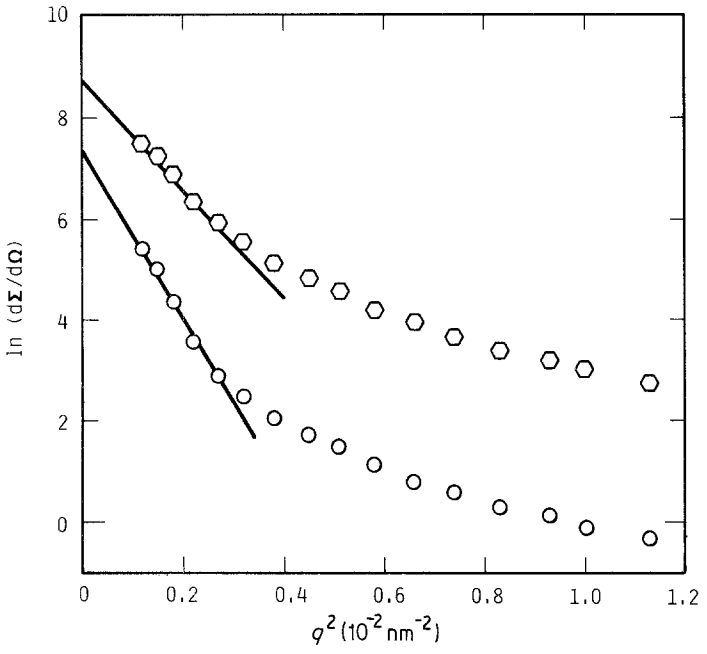

Figure 2 Plot of ln (dΣ/dΩ) against q^2 for cyclically crept samples illustrating the existence of the Guinier region at low q. The silicon carbide and alumina specimens were crept for 24 h (ε = 0.837%) and 19.8 h (ε = 3.88%), respectively. (⬡) Hot-pressed silicon carbide, (○) sintered alumina.

4. Results

The radially averaged scattering from samples subjected to cyclic creep was similar to the scattering from statically loaded samples [9, 10]. Guinier's law [23] was obeyed at small values of q, as shown in Fig. 2, and Porod's law [24] was obeyed at large values of q, as shown in Fig. 3. Because the data extended into both the Guinier and Porod regions, it was possible to determine the radius of gyration, R_G, the Porod radius, R_p, the cavity volume per unit volume, V_c/V, and the number of cavities per unit volume, N_c/V, for both the silicon carbide and the alumina samples.

4.1. Hot-pressed silicon carbide

The cavity parameters obtained from the neutron scattering measurements of the hot-pressed silicon carbide specimens subjected to cyclic creep are presented in Table I. Corresponding parameters obtained under static loading [10] have been included in Table I for comparison. The time shown in Tables I and II is the total time of the test for both static and cyclic specimens. It is worth mentioning again that the only difference between the cyclic and the static tests was the inclusion of periodic loading and unloading and a one second hold time at σ_{min}.

The most straightforward way of determining the effect of the cyclic loading component is to compare the cyclic and static behaviour using the time at σ_{max} as the normalizing parameter. For static loading, the time at σ_{max} is simply the total test duration, while for the cyclic loading used in these experiments, the time at σ_{max} is one-third of the total test duration. Using this comparison procedure, any difference in behaviour can thus be ascribed to the effect of cyclic loading.

The minimum creep rates found using the above comparison method were 2.9×10^{-7} and 2.3×10^{-7} sec^{-1} for static and cyclic loading, respectively. Similarly, the cavity volume fractions, the cavity densities, and the cavity radii are compared in Figs 4 to 6. It is obvious from these curves that when compared on the basis of time at maximum load, the cavitation behaviour, as well as the creep behaviour, of the cyclically loaded silicon carbide samples was indistinguishable from the statically loaded samples. Linear behaviour was observed in the log–log plot of cavity volume fraction against time at σ_{max} (Fig. 4) with the volume fraction being expressed as

$$\frac{V_c}{V} = 8.2 \times 10^{-6} t^{0.62} \quad (1)$$

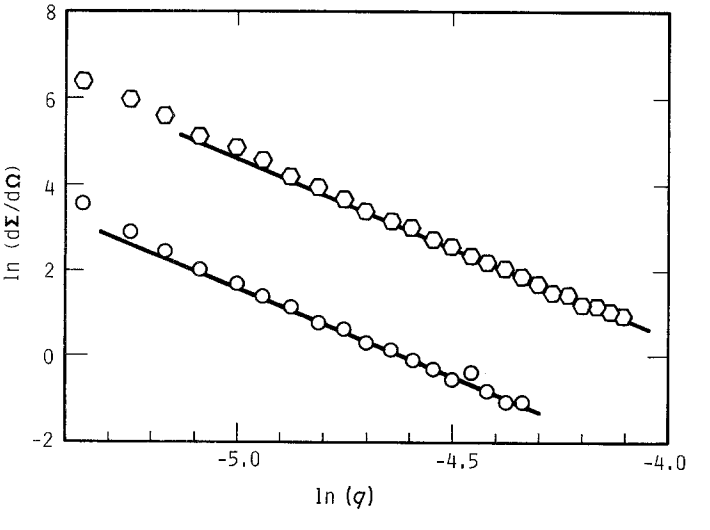

Figure 3 Plot of ln (dΣ/dΩ) against ln q illustrating Porod behaviour at high q for cyclically crept specimens. The silicon carbide and alumina specimens were crept for 24 h (ε = 0.837%) and 19.8 h (ε = 3.88%), respectively. The solid lines represent the linear fit to the data in the Porod region with a slope of −4. (⬡) Hot-pressed silicon carbide, (○) sintered alumina.

TABLE I Cavity parameters for hot-pressed silicon carbide under cyclic and static creep conditions. Static results are from Page *et al.* [10]

Maximum stress (MPa)	R	Time (h)	Strain (%)	R_G (nm)	R_p (nm)	V_c/V (10^{-3})	N_c/V ($10^{18}\,m^{-3}$)
605	0.11	0.5	0.198	48.9	53.3	0.901	1.42
605	0.11	3.0	0.367	51.6	26.2	1.00	13.3
605	0.11	6.0	0.545	53.0	36.6	1.53	7.45
605	0.11	24.0	0.837	56.4	50.9	3.59	6.48
605	0.11	48.0	1.27	58.6	59.5	5.75	6.50
605	0.11	72.0	2.51	61.1	73.2	10.1	6.13
605	1.0	0.17	0.181	49.3	33.0	0.310	2.06
605	1.0	0.75	0.523	51.8	39.5	1.82	7.05
605	1.0	3.0	0.644	49.8	34.5	2.18	12.6
605	1.0	6.0	1.15	53.9	52.4	5.18	8.62
605	1.0	12.0	1.69	53.5	52.4	6.09	10.1
605	1.0	25.0	3.10	56.3	61.8	7.77	7.87

where t is the time at maximum stress in seconds. The number of cavities per unit volume increased rapidly during the initial stages of creep (Fig. 5), reaching a density of approximately $10^{19}\,m^{-3}$ at approximately 3×10^3 sec. At this point nucleation appeared to cease, and the pore density either remained constant or decreased slightly during additional creep. Both the radius of gyration and the Porod radius were found to increase with increasing creep time (Fig. 6). The Porod radius exhibited the largest change, increasing from approximately 30 nm during the early stages of creep to approximately 60 nm during the latter stages.

4.2. Sintered alumina

The cavity parameters obtained from the neutron scattering measurements of the sintered alumina specimens subjected to cyclic creep are presented in Table II along with the previously obtained results for static loading [9]. Plots of cavity volume fraction, cavity density and radius of gyration against time at maximum load are presented in Figs 7 to 9. Although considerable sample to sample variation is present in the data, these plots suggest that the cavitation behaviour of the sintered alumina was measurably affected by the cyclic loading. Minimum creep rates under the two loading conditions were comparable, however. Based on the time at σ_{max}, the minimum creep rates for cyclic and static loading were 1.6×10^{-6} and $1.4 \times 10^{-6}\,sec^{-1}$, respectively.

As shown in Fig. 7, cyclic creep produced a slightly higher cavity volume fraction than static creep for an equivalent length of time at σ_{max}. Linear behaviour was observed for both loading conditions in log–log plots of cavity volume fraction against time at σ_{max}, with the volume fraction being expressed as

$$\frac{V_c}{V} = 3.7 \times 10^{-7} t^{0.60} \quad (2)$$

for cyclic loading, and as

$$\frac{V_c}{V} = 3.7 \times 10^{-8} t^{0.78} \quad (3)$$

for static loading, where t is the time at σ_{max} in seconds. Similarly, the cavities produced by cyclic creep were larger than those produced during static creep, as demonstrated in Fig. 9. In both cases the radius of gyration was independent of time, however, R_G was approximately 80 nm under cyclic creep and only

TABLE II Cavity parameters for sintered alumina under cyclic and static creep conditions. Static results are from Page *et al.* [9]

Maximum stress (MPa)	R	Time (h)	Strain (%)	R_G (nm)	R_p (nm)	V_c/V (10^{-5})	N_c/V ($10^{16}\,m^{-3}$)
140	0.25	0.5	0.119	81.4	94.6	2.20	0.620
140	0.25	1.0	0.070	82.1	101.4	3.61	0.824
140	0.25	3.0	0.397	81.9	101.3	2.02	0.459
140	0.25	6.0	0.914	81.7	100.5	7.93	1.86
140	0.25	12.0	1.78	80.5	93.9	8.79	2.54
140	0.25	19.8	3.88	81.7	101.1	28.7	6.65
140	1.0	0.33	0.120	62.1	66.7	0.94	0.756
140	1.0	0.33	0.260	63.5	70.3	1.07	0.735
140	1.0	1.0	0.300	62.2	57.5	2.64	3.32
140	1.0	1.0	0.800	62.1	63.2	1.50	1.42
140	1.0	3.3	0.978	61.9	64.1	4.14	3.75
140	1.0	3.3	2.70	61.7	55.8	4.47	6.14
140	1.0	6.0	1.68	62.7	71.8	7.14	4.61
140	1.0	8.8	3.38	61.6	69.4	10.7	7.64
140	1.0	10.0	1.94	62.5	70.1	12.5	8.66
140	1.0	10.0	7.52	64.9	69.5	28.2	20.1
140	1.0	10.3	7.75	60.2	59.6	14.4	16.2

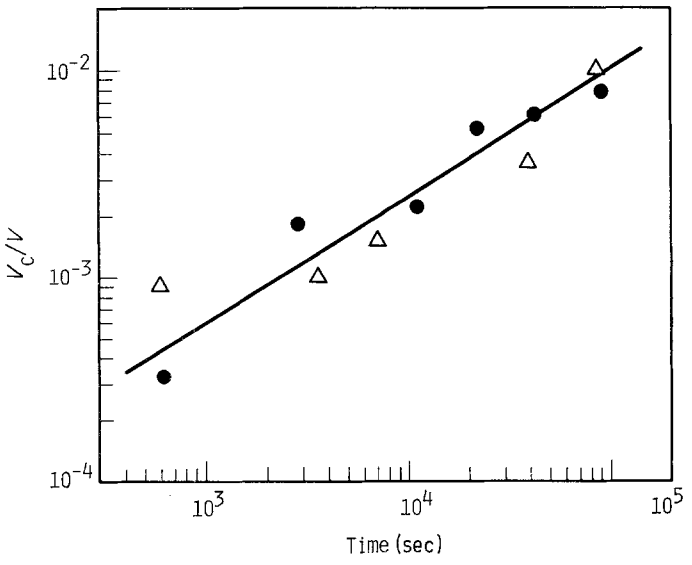

Figure 4 Cavity volume fraction against time at maximum stress for both (△) cyclic and (●) static loading of hot-pressed silicon carbide. The solid line is the fit to the static data from Page *et al.* [10].

slightly above 60 nm for static creep. The Porod radius, although not plotted, was also independent of time and larger for cyclic creep than for static creep.

Although cyclic creep produced a higher volume fraction of cavities and larger cavities, it appeared to produce a slightly lower cavity density than that observed under static creep (Fig. 8). Linear least-squares fits of the two data sets yielded the following expressions for cavity density:

$$\frac{N_c}{V} = 1.0 \times 10^{14} t^{0.59} \text{m}^{-3} \quad (4)$$

for cyclic loading, and

$$\frac{N_c}{V} = 3.1 \times 10^{13} t^{0.78} \text{m}^{-3} \quad (5)$$

for static loading.

5. Discussion

The results of this work indicate that the critical parameter controlling creep in silicon carbide exposed to periodic unloadings is not the number of loading cycles, but rather the length of time the material is under load. In other words, the cavitation parameters and the minimum strain rate observed under cyclic loading were identical to those observed under static loading when the comparison between the two loading conditions was based on the time at peak load. Because the cavitation and strain rates were unaffected by the periodic loading, it appears that the creep lifetimes of silicon carbide components that experience such periodic unloadings at similar temperatures and cyclic frequencies could be accurately estimated from more easily obtained static creep results.

However, it is possible, perhaps even likely, that cyclic loading of this and similar ceramics under certain conditions will produce cavitation whose kinetics cannot be interpreted in terms of static tests. The distinctive characteristic of these ceramics is the presence of a continuous, glassy, intergranular film, in which cavitation occurs via a viscous hole growth process [10]. In the present instance, testing was performed at a relatively high temperature, and at a relatively slow cyclic rate. Under such conditions, it is expected that cavitation would proceed in a more-or-less equilibrium fashion, i.e. it should be relatively easy for the cavities to maintain the size and density which they would achieve under an equivalent (total time at stress) static case. Indeed, Kawai *et al.* [25], measured static and cyclic fatigue lifetimes for Si_3N_4 and SiC containing glassy grain-boundary films; cycling was performed at intervals of minutes, and it was found that lives under such conditions were as predicted by static lifetime measurements. As most of these periods were probably consumed by the nucleation and growth of cavities, this would be compatible with the present findings.

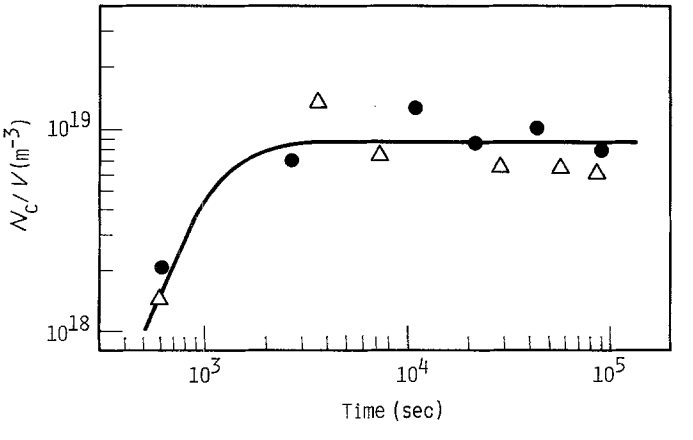

Figure 5 Number of cavities per unit volume against time at maximum stress for both (△) cyclic and (●) static loading of hot-pressed silicon carbide. The solid line is the fit to the static data from Page *et al.* [10].

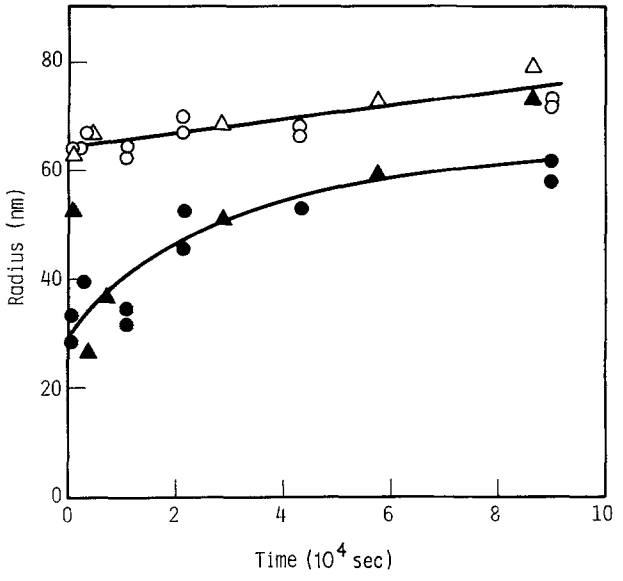

Figure 6 Cavity radius, as measured by R_G (open symbols) and R_p, (solid symbols) against time at maximum stress for both (△, ▲) cyclic and (○, ●) static loading of hot-pressed silicon carbide. The solid lines are fits to the static data from Page *et al.* [10].

Recently, however, Fett *et al.* [26], measured static and cyclic fatigue lives of hot-pressed (glassy grain-boundary) Si_3N_4 at the relatively low temperature of 1200° C, and the quite rapid frequency of 30 Hz. Under these conditions, in which the glass is expected to be highly viscous, crack growth was retarded with respect to static load predictions. Fett *et al.* [26], postulated that the retardation was related to the inability of the glassy ligaments located behind the crack tip to relax during the high-frequency cycling. Similarly, the nucleation and growth of grain-boundary cavities in the glassy phase, both of which are driven by the normal stresses across the cavitating boundary, may be markedly altered at lower temperatures and/or higher frequencies. However, in contrast to the crack growth results, cavitation is expected to increase as a result of the transient stresses.

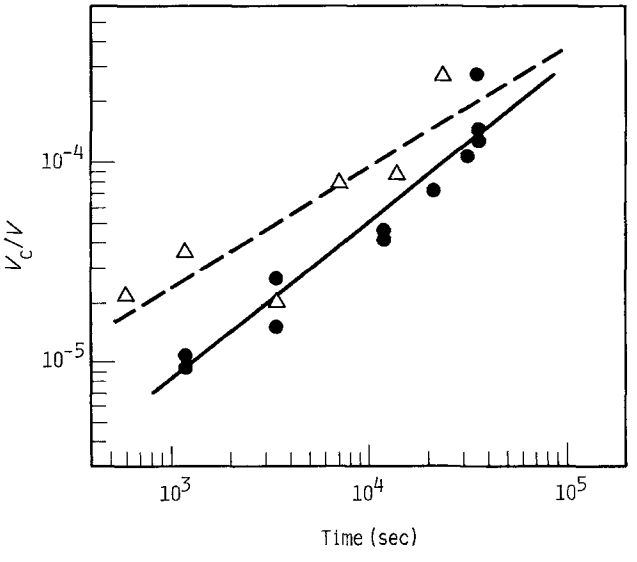

Figure 7 Cavity volume fraction against time at maximum stress for both (▲) cyclic and (●) static loading of sintered alumina. The solid and dashed lines are least-squares fits to the static and cyclic data, respectively.

In the case of the alumina material studied, the chosen test conditions were adequate to reveal clear differences in the kinetics of cavitation for cyclic versus static loading. As this ceramic possesses no intergranular film, void nucleation and growth takes place by means of grain-boundary diffusion [8, 9]. The vacancies congregate at local stress concentrations, usually grain-boundary ledges, nucleating cavities which grow until the local stress is relaxed. Weertman [27] has shown that cavities located near boundary serrations or ledges can experience stresses an order of magnitude greater than the applied stress, provided the frequency is high enough to preclude significant stress relaxation. Under these conditions, accelerated cavitation is to be expected.

In order to determine if the slightly larger cavity volume fraction and the larger cavity size obtained during cyclic creep of the alumina could be due to reduced stress relaxation, it is necessary to compare characteristic stress relaxation times with the imposed cyclic frequency. The characteristic time, t_c, for stress relaxation through grain-boundary diffusion is given by [28, 29]

$$t_c = \frac{(1 - \nu)kTL^3}{4\Omega D_b \delta_b G} \tag{6}$$

where ν is Poisson's ratio, k is Boltzman's constant, T is temperature, Ω is the atomic volume, $D_b\delta_b$ is the grain-boundary diffusivity, G is the shear modulus, and L is the characteristic diffusion length. Because of the complex nature of cavity nucleation and growth, at least three different stress concentration mechanisms, each with its own characteristic diffusion length, need be considered when estimating cyclic effects. Cavity nucleation is thought to occur at stress concentrations produced at grain-boundary ledges during boundary sliding [23]. The characteristic length for the relaxation of the stress at the ledge is the ledge height, which has been estimated [28] to be approximately 10 nm. Solving Equation 6 with the material constants listed in Table III and L = 10 nm yields a characteristic time of 3×10^{-7} sec. Raj [29] has suggested that transient stresses also can result from the presence of the cavities and from the sliding of nonplanar grain boundaries. The characteristic length for relaxation of the stress concentration due to the presence of the cavities is simply one-half of the cavity spacing, which has been estimated to be approximately 100 nm [9], while that for the grain-boundary sliding transient can be taken [29] as one-half of the grain size, which is approximately 30 μm. Solving Equation 6 with these values of L yields characteristic times of 4×10^{-5} and 1×10^3 sec for relaxation of the stress due to the presence of the cavities and due to grain-boundary sliding, respectively.

TABLE III Material constants for sintered alumina (Lucalox) at 1600° C

Constants	Values
Ω	4.2×10^{-29} m^3
$D_b\delta_b$	2.7×10^{-21} m^3 s^{-1}
G	1.182×10^5 MPa
k	1.38×10^{-23} J K^{-1}

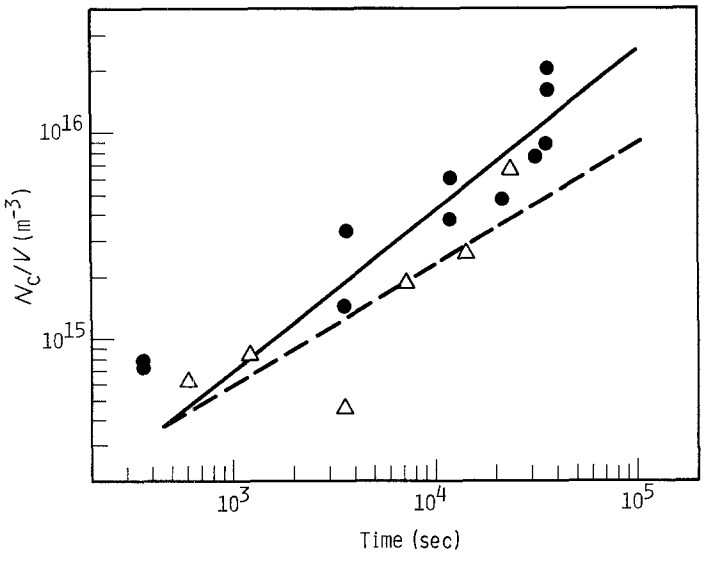

Figure 8 Number of cavities per unit volume against time at maximum stress for both (△) cyclic and (●) static loading of sintered alumina. The solid and dashed lines are least-squares fits to the static and cyclic data, respectively.

It is obvious from these characteristic times that the 0.33 Hz frequency employed in this study was far too slow to affect stress relaxation at grain-boundary ledges. One would thus not expect cavity nucleation to be significantly affected by the cycling, as was observed. The stress concentration due to the presence of the cavities also relaxes much too quickly to be affected by the 0.33 Hz cycling. The grain-boundary sliding transient, however, due to its large diffusion distance, exhibits a relaxation time that is much larger than the cycling time. It thus appears that 0.33 Hz is fast enough to limit the stress relaxation that occurs during grain-boundary sliding, and it may be through this mechanism that the cavity size and volume fraction are increased by cycling.

Although the results presented in this paper do not demonstrate dramatic effects of cyclic creep on grain-boundary cavitation, it must be remembered that the frequency employed in these tests was quite low. Studies of metallic materials [1, 7, 30] and the previously mentioned ceramic materials [25, 26] show that the cyclic effects increase at increasing frequencies. Clearly, it would be very interesting to extend the present work on cyclic cavitation in ceramics to lower temperatures and higher frequencies.

6. Conclusions

The following conclusions can be drawn from the results obtained in the present investigation.

1. Periodic unloadings coupled with short hold times at reduced load had no effect on either the cavitation rate or the minimum creep rate in a hot-pressed silicon carbide. The parameter controlling creep damage in this material was the amount of time at maximum load, rather than the number of loading cycles.

2. Periodic unloadings coupled with short holds at reduced load had a significant effect on cavitation in a sintered alumina, although no effect on the minimum creep rate. The total cavity volume fraction and the average cavity size were both increased by cyclic loading.

3. The hot-pressed silicon carbide deforms primarily by viscous creep, and it is postulated that the lack of a significant cyclic creep effect is due to the relatively high temperature and low cyclic frequency employed.

4. Estimates of diffusional relaxation times for alumina suggest that a cyclic frequency of 0.33 Hz is fast enough to retard the relaxation of stresses resulting from grain-boundary sliding, and thus facilitate cavity growth.

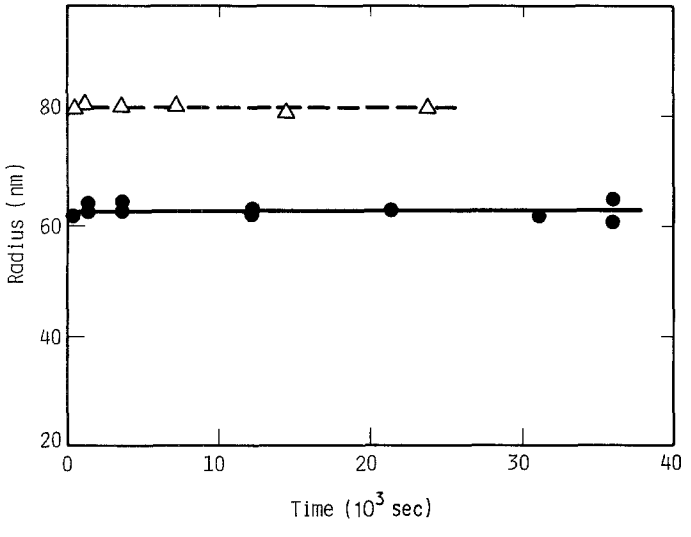

Figure 9 Cavity radius, as measured by R_G, against time at maximum stress for both (△) cyclic and (●) static loading of sintered alumina. Note that R_G is independent of time in both loading conditions.

Acknowledgements

The authors are grateful for the support of this work by the Department of Energy under Contract no. DE-FG05-84ER45063. We would also like to thank the staff of the National Center for Small-Angle Scattering Research for their assistance in this work.

Appendix. Scattering evaluation

If the measured data extend into both the Guinier [23] and Porod [24] regions, the scattering curves can be extrapolated such that the range of q from zero to infinity is covered, and thus the invariant can be evaluated. For the case of a dilute distribution of non-interacting scatterers the invariant is proportional to the total cavity volume as

$$4\pi \int_0^\infty \frac{d\Sigma}{d\Omega} q^2 \, dq = 8\pi^3 (\Delta\varrho)^2 \frac{V_c}{V} \quad \text{(A1)}$$

where $\Delta\varrho$ is the scattering length density difference between a cavity and the matrix.

Having determined the invariant, it is possible to determine the Porod radius from

$$R_p = \frac{(3/\pi) \int_0^\infty q^2 (d\Sigma/d\Omega)}{\lim_{q\to\infty} q^4 (d\Sigma/d\Omega)} \quad \text{(A2)}$$

In Equation A2 the Porod radius is equal to $\langle R^3 \rangle / \langle R^2 \rangle$, where R is the void radius and $\langle\ \rangle$ denotes an average over the ensemble.

A second measure of the size of the pores, the radius of gyration, was calculated from the slope of $\ln (d\Sigma/d\Omega)$ against q^2 in the Guinier region as

$$\ln \frac{d\Sigma}{d\Omega} = A - \frac{R_G^2}{3} q^2 \quad \text{(A3)}$$

For spherical scatters, the square of the radius of gyration is equal to $3\langle R^8 \rangle / 5\langle R^6 \rangle$. Hence, both R_p and R_G are moments which lie toward the high end of the size distribution. The Porod radius, which represents the smaller of the two, was used to calculate the number of cavities from

$$\frac{N_c}{V} = \frac{3V_c}{4\pi V R_p^3} \quad \text{(A4)}$$

References

1. R. P. SKELTON, *Philos. Mag.* **14** (1966) 563.
2. L. F. COFFIN, in "Creep-Fatigue-Environment Interactions", edited by R. M. Pelloux and N. S. Stoloff (American Institute of Mining, Metallurgical, and Petroleum Engineers, New York, 1980) pp. 1–23.
3. T. SAEGUSA, J. R. WEERTMAN, J. B. COHEN and M. ROTH, *J. Appl. Cryst.* **11** (1978) 602.
4. R. A. PAGE, J. R. WEERTMAN and M. ROTH, *Acta Metall.* **30** (1982) 1357.
5. G. G. NILSSON and M. ROTH, *Mat. Sci. Eng.* **50** (1981) 101.
6. M. H. YOO, J. C. OGLE, B. S. BORIE, E. H. LEE and R. W. HENDRICKS, *Acta Metall.* **30** (1982) 1733.
7. J. G. CABANAS-MORENO, M. S. YANG, J. R. WEERTMAN, M. ROTH, Z. H. ZHANG, G. D. WIGNALL and W. C. KOEHLER, in "Fatigue Mechanisms: Advances in Quantitative Measurement of Physical Damage", ASTM STP 811, edited by J. Lankford, D. L. Davidson, W. L. Morris, and R. P. Wei (American Society for Testing and Materials, Philadelphia, 1983) pp. 95–114.
8. R. A. PAGE and J. LANKFORD, *J. Amer. Ceram. Soc.* **66** (1983) C-146.
9. R. A. PAGE, J. LANKFORD and S. SPOONER, *J. Mater. Sci.* **19** (1984) 3360.
10. *Idem, Acta Metall.* **32** (1984) 1275.
11. R. A. PAGE and S. SPOONER, *J. Mater. Sci.* **21** (1986) 1417.
12. G. Q. WEAVER and B. A. OLSON, "High Strength Silicon Carbide for Use in Severe Environments" (Norton, Worcester, Massachusetts, 1973).
13. H. L. MARCUS and M. E. FINE, *J. Amer. Ceram. Soc.* **55** (1972) 568.
14. R. I. TAYLOR, J. P. COAD and R. J. BROOK, *ibid.* **57** (1974) 539.
15. W. C. JOHNSON and D. F. STEIN, *ibid.* **58** (1975) 485.
16. R. I. TAYLOR, J. P. COAD and A. E. HUGHES, *ibid.* **59** (1976) 374.
17. W. C. JOHNSON, *Met. Trans. A* **8A** (1977) 1413.
18. *Idem, J. Amer. Ceram. Soc.* **61** (1978) 234.
19. A. H. HEUER, N. J. TIGHE and R. M. CANNON, *ibid.* **63** (1980) 53.
20. D. R. CLARKE, *ibid.* **63** (1980) 339.
21. P. E. C. FRANKEN and A. P. GEHRING, *J. Mater. Sci.* **16** (1981) 384.
22. R. W. HENDRICKS, J. SCHELTEN and W. SCHMATZ, *Philos. Mag.* **30** (1974) 819.
23. A. GUINIER, *Ann. Phys. Paris* **12** (1939) 161.
24. G. POROD, *Kolloid Z.* **125** (1952) 51.
25. M. KAWAI, H. FUJITA, Y. KANKI, H. ABE and J. NAKAYAMA, "Tensile Testing of Sintered Silicon Carbide and Silicon Nitride" (unpublished Asahi Glass Co. Report, 1983).
26. T. FETT, G. HIMSOLT and D. MUNZ, *Adv. Ceram. Mater.* **1** (1986) 179.
27. J. R. WEERTMAN, *Can. Metall. Quart.* **18** (1979) 73.
28. K. S. CHAN, R. A. PAGE and J. LANKFORD, *Acta Metall.* **34** (1986) 2361.
29. R. RAJ, *Metall. Trans. A* **6A** (1975) 1499.
30. A. GITTINS, *Metal. Sci.* **2** (1968) 51.

Received 21 August
and accepted 9 October 1986